Journal of Solid State Electrochemistry (2018) 22:2811–2820
https://doi.org/10.1007/s10008-018-3975-2

ORIGINAL PAPER

Effects of Nb substitution on structure and electrochemical properties of $LiNi_{0.7}Mn_{0.3}O_2$ cathode materials

Zhifeng Li[1] · Chuiyi Luo[1] · Chunxiang Wang[1] · Guoxiang Jiang[1] · Jun Chen[1] · Shengwen Zhong[1] · Qian Zhang[1] · Dong Li[1]

Received: 1 February 2018 / Revised: 27 March 2018 / Accepted: 20 April 2018 / Published online: 23 May 2018

Abstract

Nb-doped cathode materials with the formula $Li(Ni_{0.7}Mn_{0.3})_{1-x}Nb_xO_2$ ($x = 0$, 0.01, 0.02, 0.03, 0.04) have been prepared successfully by calcining the mixtures of $LiOH{\cdot}H_2O$, Nb_2O_5, and $Ni_{0.7}Mn_{0.3}(OH)_2$ precursor formed through a simple continuous co-precipitation method. The effects of Nb substitution on the crystal structure and electrochemical properties of $LiNi_{0.7}Mn_{0.3}O_2$ were studied systematically by X-ray diffraction (XRD), scanning electron microscope (SEM), X-ray photoelectron spectroscopy (XPS), and various electrochemical measurements. The results show that the lattice parameters of the Nb substitution $LiNi_{0.7}Mn_{0.3}O_2$ samples are slightly larger than that of pure $LiNi_{0.7}Mn_{0.3}O_2$, and the basic α-$NaFeO_2$ layered structure does not change with the Nb doping. What's more, better morphology, lower resistance, and good cycle stability were obtained after Nb substitution. In addition, CV test exhibits that Nb doping results in lower electrode polarization and XPS results indicate that the valence of Mn kept constant but the component of Ni^{3+} decreased after doping. All the results indicate that Nb doping in $LiNi_{0.7}Mn_{0.3}O_2$ is a promising method to improve the properties of Ni-rich lithium-ion batteries positive-electrode materials.

Keywords Lithium-ion batteries · Ni-rich positive-electrode materials · Niobium doping · Electrochemical properties

Introduction

In recent years, lithium-ion batteries have received intense attention as the power source in hybrid electric vehicles (HEVs), plug-in hybrid electric vehicles (PHEVs), and full electric vehicles (EVs) among the currently available energy storage technologies due to their high energy density, long cycle life, and environment friendly [1, 2]. However, the traditional lithium-ion batteries commonly based on layered $LiCoO_2$, $LiMn_2O_4$, and $LiFePO_4$ can hardly fulfill the requirement of high-power applications. Thus, design and develop alternative positive-electrode materials with higher capacity, longer cycle life, and lower cost are one of the key challenges for lithium-ion batteries.

Due to its higher energy density than traditional cathode materials, more and more researchers focus their attention on Ni-rich cathode materials, such as $LiNi_{0.8}Co_{0.15}Al_{0.05}O_2$ (NCA), $LiNi_{0.6}Mn_{0.2}Co_{0.2}O_2$ (622), $LiNi_{0.7}Mn_{0.15}Co_{0.15}O_2$, $LiNi_{0.8}Mn_{0.1}Co_{0.1}O_2$ (811), and $LiNi_xMn_{1-x}O_2$ ($x \geq 0.6$) [2]. Some of them have been applied in lithium-ion battery (LIB) systems as novel and promising positive-electrode materials. Unfortunately, their cycling and thermal stability are not satisfactory, further research is very urgent [3–5, 10, 17]. According to researchers'previous work, doping with small amounts of elements, such as Mo^{6+} [6], Al^{3+} [7], Cr^{3+} [8, 9], Mg^{2+} [8, 15, 16, 18], Fe^{3+} [11, 13], K^+ [12], Zr^{4+} [14], Ti^{4+} [19, 20], is considered as an effective way to improve the electrochemical performance of Ni-rich cathode materials. Recent research progresses proved that Nb has become one of the most attractive candidates as doping elements since it can enhance the structural stability and electrical conductivity of cathode materials [21, 30]. Yi et al. [22, 23] reported that Nb-doped $LiMn_{1.5}Ni_{0.5}O_4$ can decrease the charge transfer resistance of $LiMn_{1.5}Ni_{0.5}O_4$ and improve the rate performance. Wu et al. [24] synthesized $LiNi_{1/3}Co_{1/3}Mn_{1/3}O_2$ and the high cutoff voltage performance was improved by Nb doping. Also, the electrochemical properties are significantly enhanced in lithium-rich layered cathode materials through niobium (Nb) doping [25], and corresponding theoretical calculations verify the

✉ Shengwen Zhong
jxustzsw@126.com

[1] Jiangxi Key laboratory of Power Battery and Material, School of Materials Science and Engineering, Jiangxi University of Science and Technology, Ganzhou 341000, People's Republic of China

results [26, 27]. However, the influence of Nb doping on structure and electrochemical properties of $LiNi_{0.7}Mn_{0.3}O_2$ cathode materials have rarely been investigated.

In this paper, Nb-doped $LiNi_{0.7}Mn_{0.3}O_2$ was synthesized by calcining the mixtures of $LiOH{\cdot}H_2O$, Nb_2O_5, and $Ni_{0.7}Mn_{0.3}(OH)_2$ precursor from a simple continuous co-precipitation method and the impact of Nb substitution on structure, charge transfer resistance, valence state of Ni and Mn, and electrochemical properties were mainly discussed.

Experimental

Material preparation

Nb-doped $Li[Ni_{0.7}Mn_{0.3}]_{1-x}Nb_xO_2$ ($x = 0$, 0.01, 0.02, 0.03, 0.04) cathode materials have been prepared successfully by calcining the mixtures of $LiOH{\cdot}H_2O$, Nb_2O_5, and $Ni_{0.7}Mn_{0.3}(OH)_2$ precursor from a simple continuous co-precipitation method. Stoichiometric amounts of $NiSO_4{\cdot}$

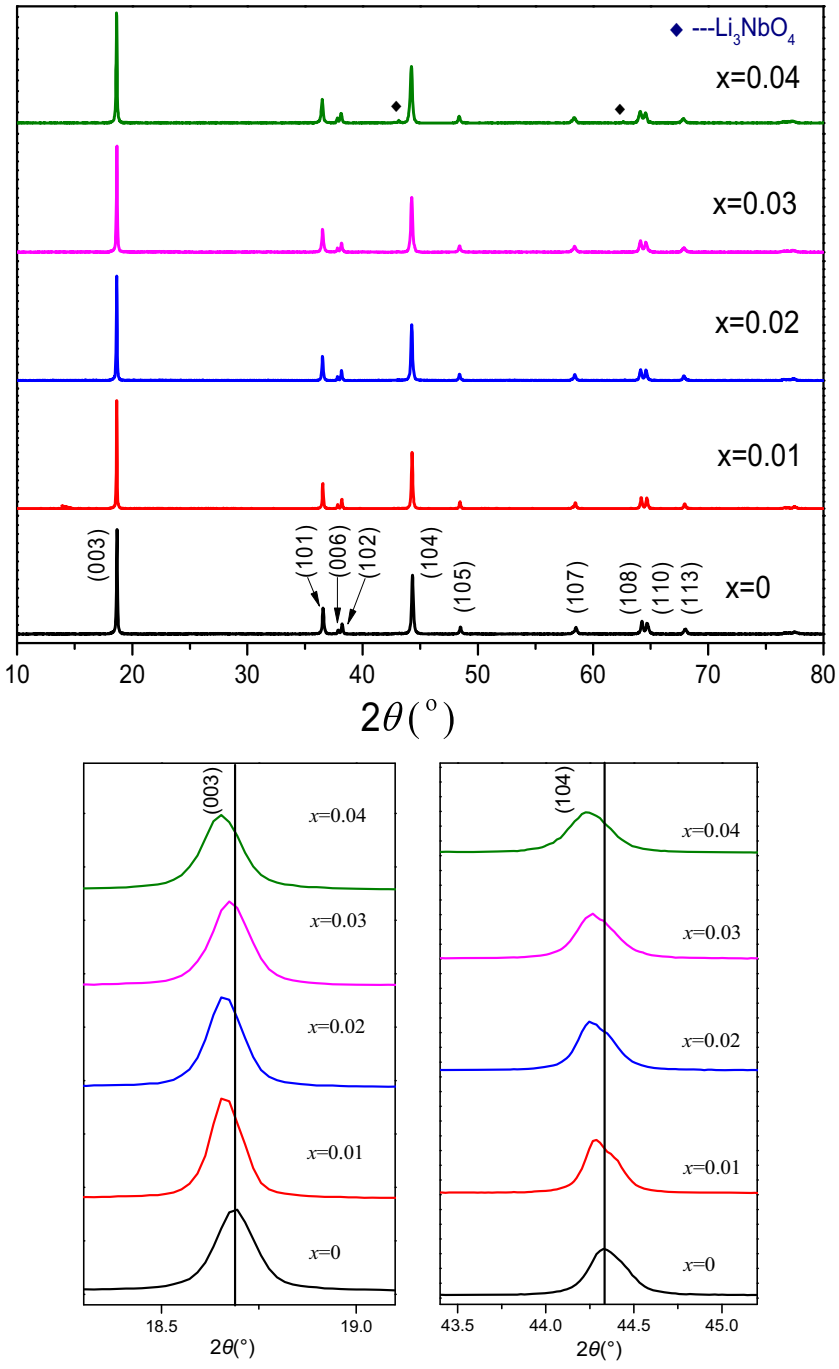

Fig. 1 XRD patterns of the prepared $Li[Ni_{0.7}Mn_{0.3}]_{1-x}Nb_xO_2$ ($x = 0$, 0.01, 0.02, 0.03, 0.04) materials

$6H_2O$ and $MnSO_4 \cdot H_2O$ were dissolved in deionized water to form 2.0 mol/L mixed solutions of Ni and Mn. In the same way, 4 mol/L NaOH solution and proper amount of $NH_3 \cdot H_2O$ solution were added to form the mixed alkaline solutions. Metal hydroxide precursors $Ni_{0.7}Mn_{0.3}(OH)_2$ were prepared via co-precipitation in a continuously stirred tank reactor under 55 °C solutions, N_2 atmosphere, and the pH of 11.2 ± 0.1. After the completion of the reaction, the resulting suspension was washed with distilled water several times and dried in an oven at 100 °C for about 24 h. Finally, the $Li[Ni_{0.7}Mn_{0.3}]_{1-x}Nb_xO_2$ ($x = 0$, 0.01, 0.02, 0.03, 0.04) cathode materials were obtained by calcining the mixtures of the hydroxide precursors, proper amount of Nb_2O_5, and 10% excess amount of $LiOH \cdot H_2O$ (to compensate for lithium loss during the high-temperature calcination process [28]) at 550 °C for 6 h, subsequently at 820 °C for 15 h under flowing air condition.

Material characterization

The structures of the samples were characterized by X-ray diffraction (Bruker D8 Advance, Cu-Kα radiation with a step of 0.02° at 40 kV and 40 mA). X-ray Rietveld refinement was performed with Reflex programs. The morphology and particle size of $Li[Ni_{0.7}Mn_{0.3}]_{1-x}Nb_xO_2$ ($x = 0$, 0.01, 0.02, 0.03, 0.04) were investigated with scanning electron microscopy (ZEISS EVO/MA10 with an accelerating voltage of 20 kV). The TEM images were obtained by a transmission electron microscope (FEI Tecnai G2 F20). In addition, the corresponding sample was dispersed into ethanol and transferred onto a Cu grid with holey carbon foil, then dried for TEM observation. Cyclic voltammetry (CV) of the cells were collected at room temperature on Ivium-n-Stat electrochemical workstation between 2.5 and 4.6 V with the scan rate of 0.1 mV s^{-1}. EIS measurements were carried out in the same electrochemical station with 10 mV AC signal and a frequency range from 10^5 to 0.001 Hz. Charge-discharge performance was characterized galvanostatically in the voltage range of 2.75–4.35 V using a NEWARE cell test instrument at room temperature.

Battery preparation

The electrochemical performances of all samples were measured in the CR2032 coin-type half-cells. The cathode active materials slurry was prepared by mixing cathode material powders with Super P carbon black and polyvinylidene fluoride (PVDF) with a weight ratio of 90:4:6 in N-methyl-2-pyrrolidine (NMP) at room temperature. The slurry was stirred overnight and coated onto aluminum foil, then dried thoroughly at 120 °C. The resulting electrode film was subsequently pressed and punched into pellets and dried in a vacuum chamber at 60 °C for 12 h. Coin cells were assembled in an argon-filled glove box with 1 M $LiPF_6$ in a mixture of ethylene carbonate (EC) and diethyl carbonate (DEC) as the electrolyte solution, and Celgard 2300 polypropylene was employed as the separator.

Results and discussion

XRD phase

The results of X-ray diffraction patterns of the prepared $Li[Ni_{0.7}Mn_{0.3}]_{1-x}Nb_xO_2$ ($x = 0$, 0.01, 0.02, 0.03, 0.04) materials are respectively shown in Fig. 1. All samples could be indexed by a hexagonal α-$NaFeO_2$ structure [29]. The slight split of (006)/(102) and (108)/(110) indicates that the products possess typical layered structure characteristics [30]. However, there is some impurity phase of Li_3NbO_4 in the patterns of $Li[Ni_{0.7}Mn_{0.3}]_{0.96}Nb_{0.04}O_2$, meaning that Nb^{5+} do not completely substitute Ni(Mn) 3*a* site. Moreover, with the *x* increase (*x* from 0 to 0.02), the (003) and (104) diffraction peaks slightly shift to lower 2θ, which means the interlayer spacing is extended after doping with Nb^{5+}, so the diffusion coefficient of Li^+ may increase [31].

Lattice constants shown in Table 1 were obtained by Rietveld refinement method and the results of X-ray diffraction patterns are illustrated in Fig. 1. The little difference between the experimental and calculated patterns and the low values of R_{wp} demonstrated that these were successful refinements. The lattice constant *a* and *c* and

Table 1 Lattice parameters of $Li[Ni_{0.7}Mn_{0.3}]_{1-x}Nb_xO_2$ ($x = 0$, 0.01, 0.02, 0.03, 0.04) samples obtained from Rietveld refinement of the XRD patterns

Samples	*a*/Å	*c*/Å	*c*/*a*	*I*(003)/I(004)	*V*/Å^3	R_{wp} (%)
$x = 0$	2.8788(6)	14.2439(4)	4.9477	1.9076	102.24	5.83
$x = 0.01$	2.8806(3)	14.2601(6)	4.9504	2.0981	102.48	5.68
$x = 0.02$	2.8830(2)	14.2634(5)	4.9474	2.0724	102.67	5.63
$x = 0.03$	2.8832(9)	14.2556(3)	4.9442	2.0629	102.64	6.52
$x = 0.04$	2.8856(4)	14.2703(9)	4.9453	2.0419	102.91	5.81

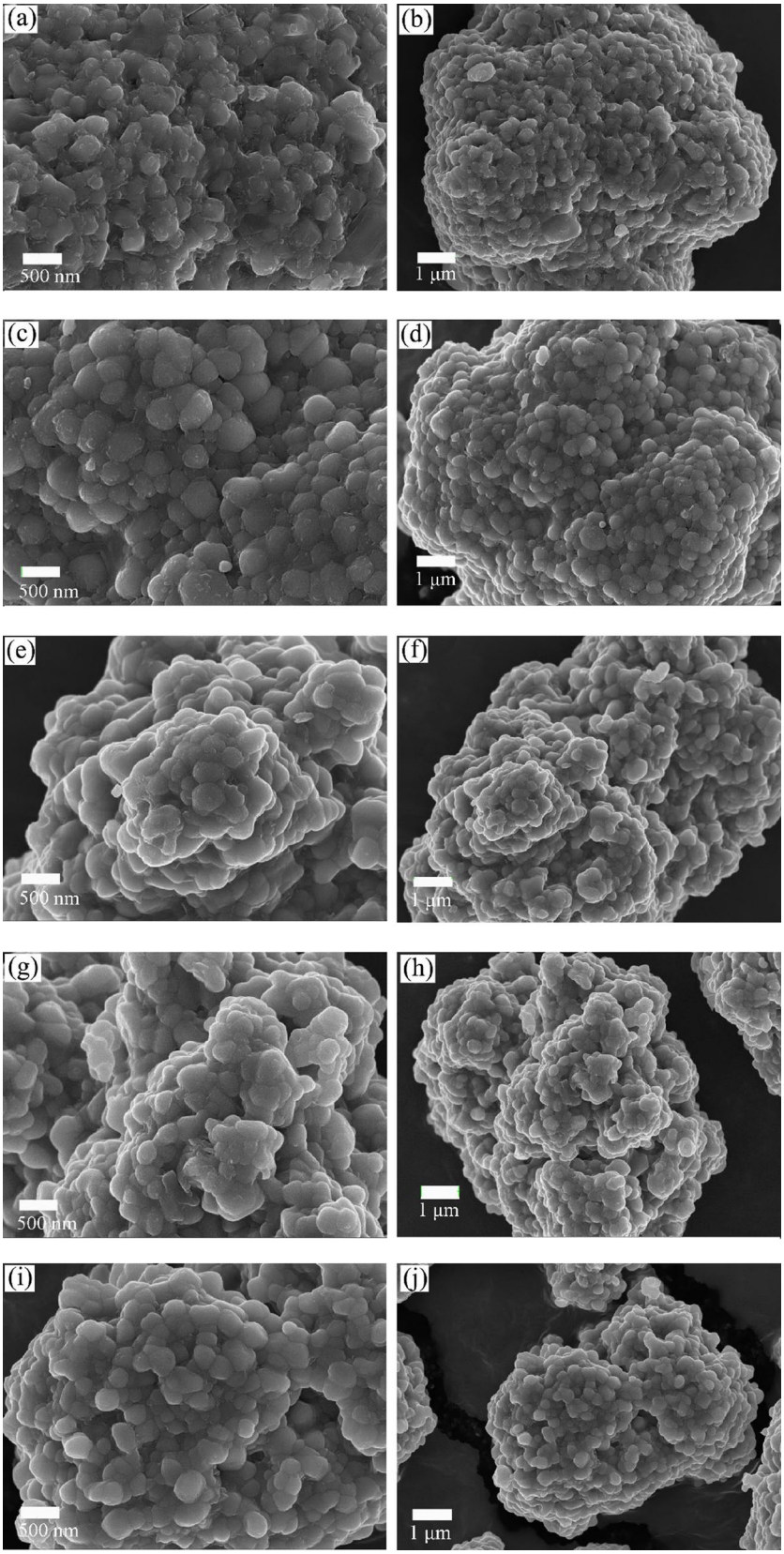

Fig. 2 SEM images of $LiNi_{0.7}Mn_{0.3}O_2$ (**a**, **b**), $Li[Ni_{0.7}Mn_{0.3}]_{0.99}Nb_{0.01}O_2$ (**c**, **d**), $Li[Ni_{0.7}Mn_{0.3}]_{0.98}Nb_{0.02}O_2$ (**e**, **f**), $Li[Ni_{0.7}Mn_{0.3}]_{0.97}Nb_{0.03}O_2$ (g, h) and $Li[Ni_{0.7}Mn_{0.3}]_{0.96}Nb_{0.04}O_2$ (**i**, **j**)

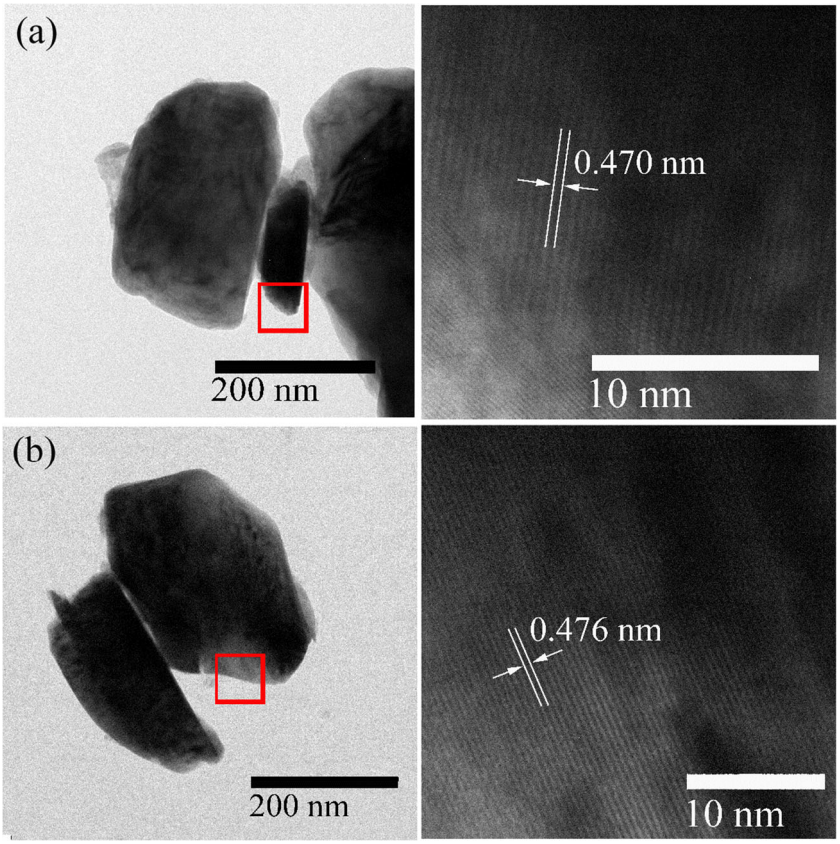

Fig. 3 Images of $LiNi_{0.7}Mn_{0.3}O_2$ materials. **a** Undoped. **b** Doped with 2% Nb

cell volume *V* expand regularly with the Nb-doping content increase, which is close to the results reported by Wu et al. [24]. This is attributed to the larger Nb^{5+} (0.64 Å) substitutes Ni^{3+} (0.56 Å) and Mn^{4+} (0.53 Å) sites. However, the change of cell parameters begins irregularly with the further increase of Nb content, which mainly because of the Nb^{5+} react with Li^+ to form a new Li_3NbO_4 phase. According to the reports before [32], the integrated intensity ratio of (003) and (104) peaks (*I*(003)/I(104)) and the value of *c*/*a*, are regarded as an important index of the cation mixing. The larger *I*(003)/I(104) and *c*/*a* value, the lower Li^+-Ni^{2+} ion mixing in the doped samples. Nb substitution has improved the crystallinity of $LiNi_{0.7}Mn_{0.3}O_2$.

Microtopography

The SEM images of $Li[Ni_{0.7}Mn_{0.3}]_{1-x}Nb_xO_2$ ($x = 0$, 0.01, 0.02, 0.03, 0.04) samples are shown in Fig. 2. Compared with the undoped sample, the particles of all the Nb substitution samples are made up of abundant small primary grains. This may increase the electrode-electrolyte contact area and facilitate the lithium-ion transportation, and then improve the electrochemical performance. But the average particle size of Nb substitution samples is about 10 μm, which was roughly same as the $LiNi_{0.7}Mn_{0.3}O_2$ sample. The spherical morphologies are similar with Li's [25] report.

To further investigate the changes in microstructure and morphology for the $LiNi_{0.7}Mn_{0.3}O_2$ electrodes before and after Nb doping, TEM and HRTEM images were recorded as shown in Fig. 3. HRTEM images with different lattice spacing were detected and assigned to the {003} plane. Compared with the undoped samples, the lattice spacing of the samples doped by 2% Nb was 0.476 nm, which was slightly larger than the value of the undoped sample (0.470 nm). Nb doping made the lattice slightly expand in the c axis direction and increased the lattice spacing, which would be more conducive to the transmission of lithium ions. This conclusion was in agreement with the results discussed in the section on the XRD investigation.

Electrochemical performance

Cyclic voltammetry (CV) is a useful electrochemical tool to study the redox behavior in an electrochemical reaction. Figure 4 shows cyclic voltammograms of $Li[Ni_{0.7}Mn_{0.3}]_{1-x}Nb_xO_2$ ($x = 0$, 0.01, 0.02, 0.03, 0.04) electrodes between 2.75 and 4.6 V with a scanning rate of 0.1 mV s^{-1}, and

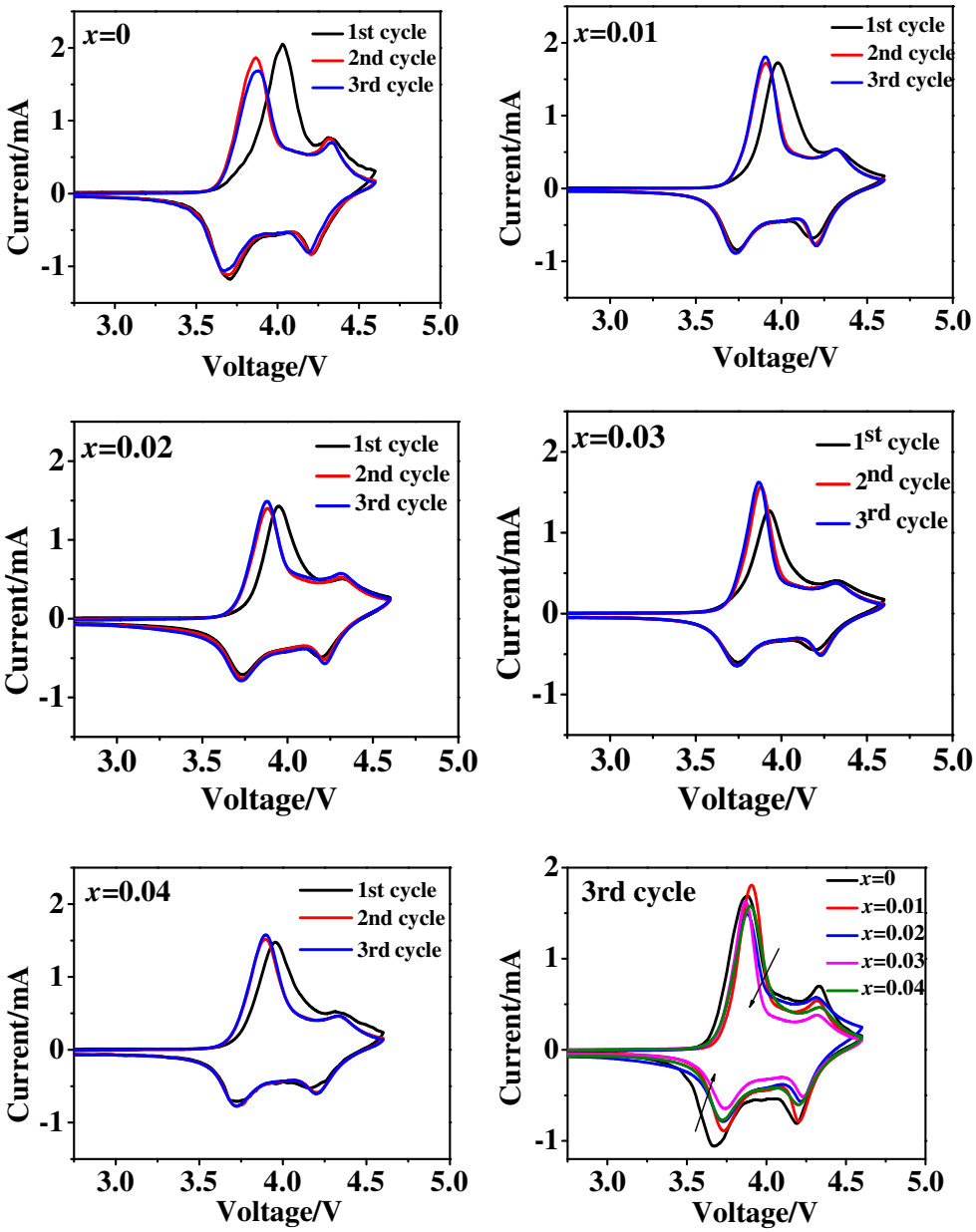

Fig. 4 Cyclic voltammograms of $LiNi[_{0.7}Mn_{0.3}]_{1-x}Nb_xO_2$ ($x = 0$, 0.01, 0.02, 0.03, 0.04) materials at a scan rate of 0.1 mV/s

values of the third cycle CV peak are listed in Table 2. The redox peaks mainly located near 3.9 V are ascribed to the oxidation/reduction of Ni^{2+}/Ni^{4+}or Ni^{3+}/Ni^{4+}, and small redox peaks appear near 4.3 V can be attributed to the phase transition of hexagonal to hexagonal (H2 to H3) for Ni-rich layered compounds [32, 34]. The first cycle is different from the subsequent ones due to the mechanism of initial activation and stabilization which forming a solid electrolyte inter-phase [33, 34] or the cation mixing [35]. Compared to the undoped sample, Nb-substituted samples exhibit less potential difference between anodic peak and cathodic peak ($^{\triangle}\psi V$) showed in Table 2. All these results manifest that Nb substitution could reduce electrode polarization.

The initial charge/discharge curves and the capacity data of all the samples are shown in Fig. 5a and Table 3, respectively. It can be seen that the initial charge capacity of

Table 2 Values of the CV peaks for $LiNi[_{0.7}Mn_{0.3}]_{1-x}Nb_xO_2$ ($x = 0$, 0.01, 0.02, 0.03, 0.04) materials

samples	ψ1/V	ψ2/V	$\Delta\psi$12/mV	ψ3/V	ψ4/V	$\Delta\psi$34/mV
$x = 0$	3.881	3.670	221	4.329	4.191	138
$x = 0.01$	3.907	3.731	176	4.317	4.203	114
$x = 0.02$	3.878	3.732	146	4.309	4.219	90
$x = 0.03$	3.868	3.741	127	4.314	4.231	83
$x = 0.04$	3.898	3.723	175	4.336	4.203	133

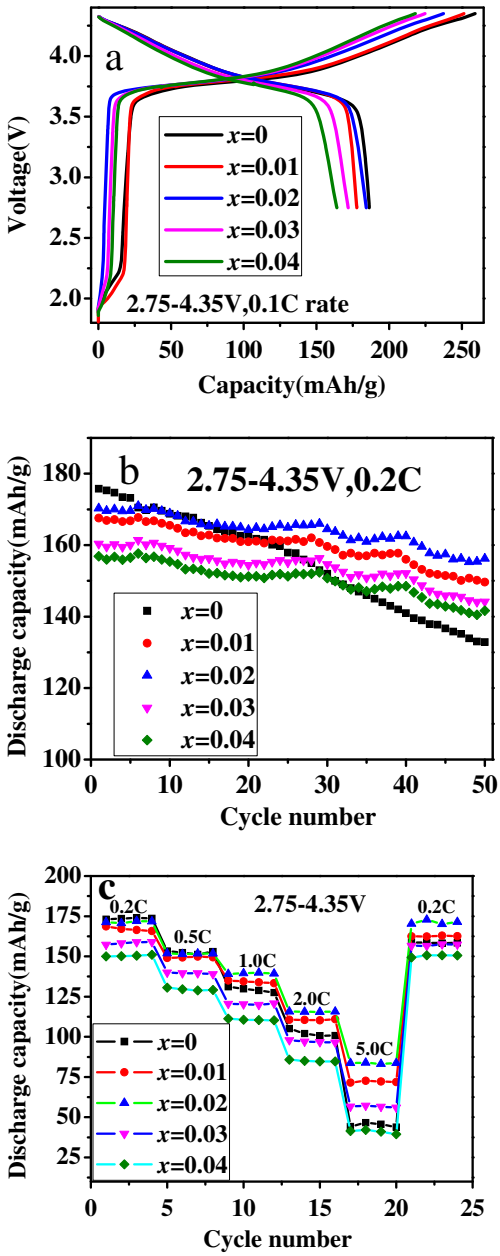

Fig. 5 **a** Initial charge-discharge capacity curves of all samples. **b** Cycling performance of all samples. **c** Rate performance of all samples

$LiNi_{0.7}Mn_{0.3}O_2$ is 259.12 mAh/g, approaching their theoretical values of 274 mAh/g. However, with the increasing Nb doping, the initial discharge capacity decreased. As illustrated in Table 3, the electrodes with $x = 0$, 0.01, 0.02, 0.03, and 0.04 deliver discharge capacities of 179.78, 184.32, 170.85, and 164.03 mAh/g, severally.

Figure 5b shows the cycling performance of $Li[Ni_{0.7}Mn_{0.3}]_{1-x}Nb_xO_2$ ($x = 0$, 0.01, 0.02, 0.03, 0.04) samples operated between 2.75 and 4.35 V at 0.2 C. The discharged capacity of pristine sample and Nb-doped sample (1, 2, 3, 4%) at the 50th cycle are 133.2, 150.6, 156.3, 144.2, and 141.7 mAh/g, respectively, which corresponds to capacity retention of 75.8, 90.0, 91.8, 89.9, and 88.3%. Therefore, Nb substitution could improve the cycle performance effectively.

The rate capability test results for the $Li[Ni_{0.7}Mn_{0.3}]_{1-x}Nb_xO_2$ ($x = 0$, 0.01, 0.02, 0.03, 0.04) cells are shown in Fig. 5c. Due to the internal polarization of lithium intercalation/deintercalation reaction, the discharge capacity of all electrode materials gradually decreased with the current density increased [36]. It is easy to find that the $x = 0.02$ sample exhibits better performance than $x = 0$ sample, especially at high rates. While the $x = 0.04$ sample manifests worse rate property due to the impurity Li_3NbO_4 phase in material. The expanded Li^+ channels and the facilitated migration of Li^+ ions in Nb^{5+} substitution samples ($x = 0.01$, 0.02, 0.03) contribute to the good rate performance. These results are consistent with the expectation from previous lattice analysis.

In order to investigate the internal resistance change between the 4th cycle and the 50th cycle, electrochemical impedance spectroscopy measurement (EIS) technology was applied; the EIS profiles are demonstrated in Fig. 6a, b, respectively. R_s, R_{sf}, and R_{ct} calculated from EIS results are tabulated in Table 4. According to the reported references [24, 32], the symbols R_s, R_{sf}, R_{ct}, and Z_w represent the ohmic resistance between the working electrode and the reference electrode, the resistance for Li^+ diffusion in the surface layer, the charge transfer resistance, and the Warburg impedance of solid phase diffusion, respectively. Obviously, the resistance for Li^+ diffusion in the surface layer (R_{sf}) and the charge transfer resistance (R_{ct}) of Nb-doped samples are very close to each other in Fig. 6 which is much smaller than $LiNi_{0.7}Mn_{0.3}O_2 (x = 0)$. It reveals that the ionic conductivity was improved greatly by Nb doping and this is the reason of good electrochemical performance obtained before.

XPS analysis

As discussed above, $LiNi[_{0.7}Mn_{0.3}]_{1-x}Nb_xO_2$ materials with the $x = 0.02$ show the best electrochemical performance. To

Table 3 Initial charge-discharge capacity data of all the samples proceed at 0.1 C

Samples	Initial charge capacity (mAh/g)	Initial discharge capacity (mAh/g)	Irreversible capacity (mAh/g)	Columbic efficiency/ %
$x = 0$	259.12	185.33	73.79	71.5
$x = 0.01$	249.43	179.78	69.65	72.1
$x = 0.02$	237.37	184.32	53.05	77.6
$x = 0.03$	224.62	170.85	53.77	76.1
$x = 0.04$	217.99	164.03	53.96	75.2

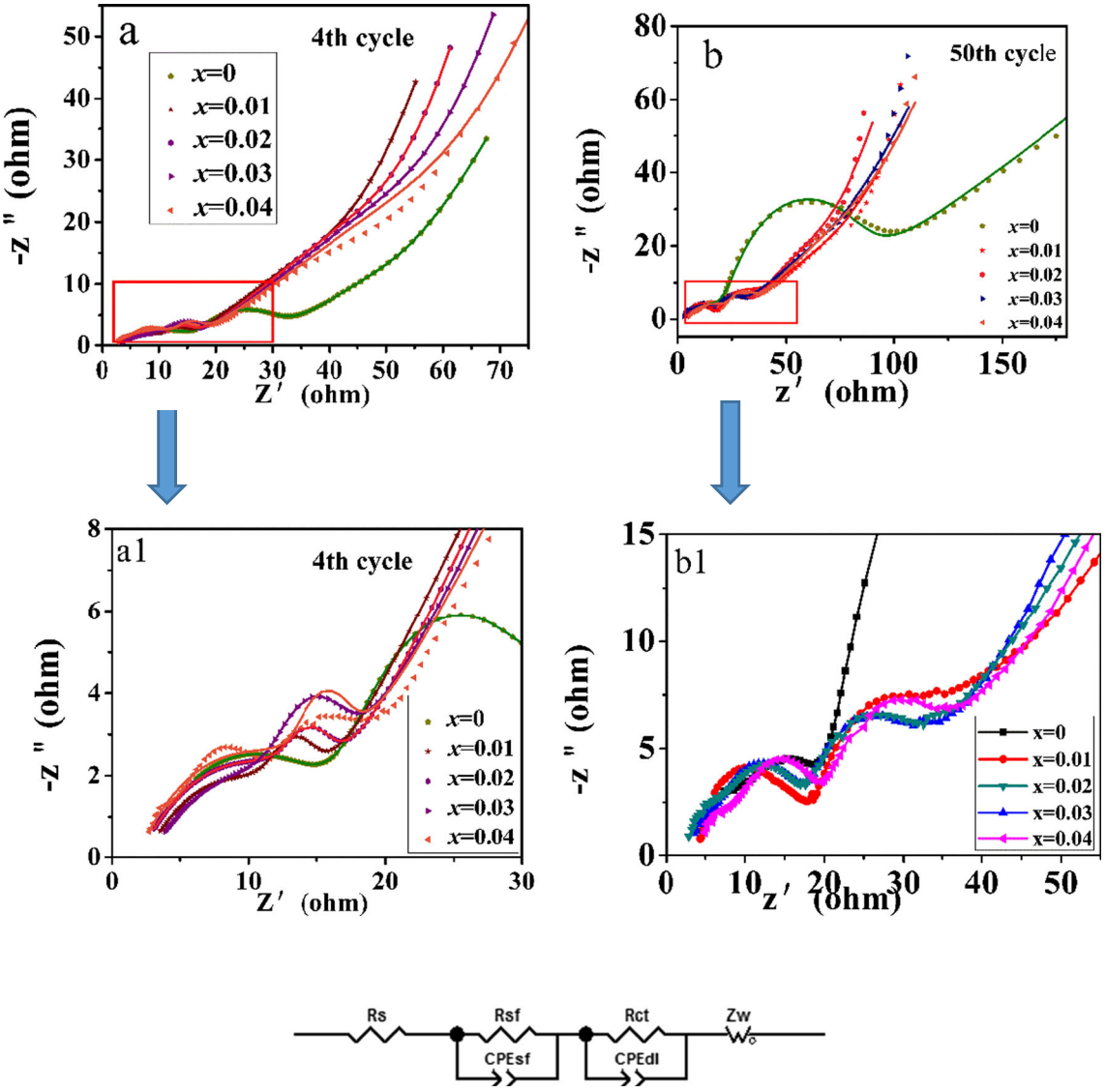

Fig. 6 Nyquist plots and equivalent circuit for $LiNi[_{0.7}Mn_{0.3}]_{1-x}Nb_xO_2$ ($x = 0$, 0.01, 0.02, 0.03, 0.04) positive-electrode materials at charge state of 4.0 V after 4 cycles, the scatters represent the experimental data and the continuous lines represent the fitted data

Table 4 The fitting results of EIS after the 4th and 50th cycle

Cycle times	Samples	R_s (Ω)	R_{sf} (Ω)	R_{ct} (Ω)
4th cycle	$x = 0$	6.156	8.986	18.1
	$x = 0.01$	4.523	4.579	6.747
	$x = 0.02$	3.965	5.086	7.499
	$x = 0.03$	3.816	5.917	8.14
	$x = 0.04$	4.857	4.666	8.384
50th cycle	$x = 0$	6.121	11.95	72.04
	$x = 0.01$	5.158	11.76	18.35
	$x = 0.02$	5.085	10.67	16.25
	$x = 0.03$	4.159	11.59	16.52
	$x = 0.04$	4.518	10.82	18.37

gain more insights into the oxidation state of transition metals in the layered $LiNi_{0.7}Mn_{0.3}O_2$ material and $x = 0.02$ sample, X-ray photoelectron spectroscopy (XPS) were recorded as shown in Fig. 7. The Ni 2p spectra were composed of two main peaks, Ni2p 3/2 (855.52 eV) and Ni2p 1/2 (873 eV), which was attributed to Ni^{3+} ions based on the simple ionic model [37], but another small peak, Ni2p 3/2 (854.39 eV) was corresponding to Ni^{2+}. The Ni was with the mixing valence states. More importantly, the relative peak area ratios of Ni^{3+}/Ni^{2+} before and after doping were 7.7040 and 4.9575, respectively, meaning that the Ni^{3+} component gradually decreased, whereas the growth of the Ni^{2+} component at 854.39 eV became evident. The binding energy of Mn2p 3/2 was about 642.2 eV, in agreement with the value reported for MnO_2 [38] in both two samples. The result indicated that the

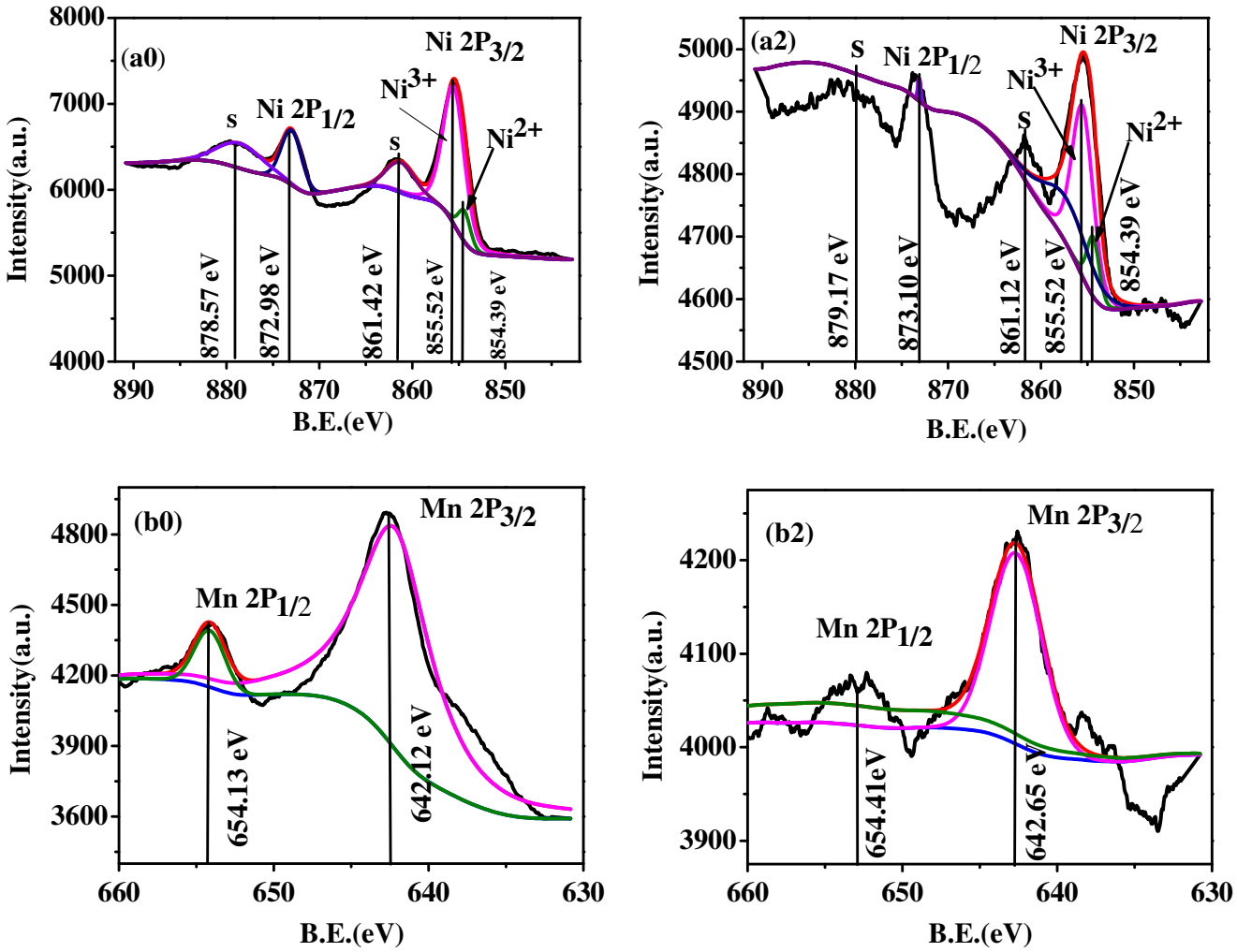

Fig. 7 XPS spectra of Ni 2p (a0, a1), Mn 2p (b0, b1) of the pristine $LiNi_{0.7}Mn_{0.3}O_2$, 2% doped-$LiNi_{0.7}Mn_{0.3}O_2$ materials (XPS spectra of a0, b0 refer to pristine sample; a2, b2 refer to 2% doped sample)

oxidation valence of Mn was kept constant in tetravalent, only Ni changed after doping.

Conclusion

$Li(Ni_{0.7}Mn_{0.3})_{1-x}Nb_xO_2$ ($x = 0, 0.01, 0.02, 0.03, 0.04$) cathode materials have been prepared successfully by calcining the mixtures of $LiOH{\cdot}H_2O$, Nb_2O_5, and $Ni_{0.7}Mn_{0.3}(OH)_2$ precursor formed through a simple continuous co-precipitation method. The effect of Nb substitution on the structure, morphology, and electrochemical properties of $LiNi_{0.7}Mn_{0.3}O_2$ was investigated in detail. The results indicate that Nb substitution has an effective effect on the improvement of cycling performance of $LiNi_{0.7}Mn_{0.3}O_2$. Moreover, Nb substitution could decrease the electrode polarization and the 2% Nb-doped sample has the lowest charge transfer impedance, best cycling performance at 0.2 C under the potential of 2.75–4.35 V among all the doped samples. In the end, X-ray photoelectron spectroscopy (XPS) indicated that the Mn were kept tetravalent but Ni was in + 2 and + 3 mixing valence states and Ni^{3+} component decreased after doping. This study will be helpful for improving the cycle performance of cobalt-free Ni-rich cathode materials.

Funding information This work received financial support from the National Natural Science Fund of China (No. 51372104), Jiangxi Province Science and Technology Plan Project (grant nos. 20141BBE50019, 20151BBE50106), Youth science fund program of Jiangxi science and technology bureau (grant no. 2010GQC0064), and Jiangxi Provincial Education Office Natural Science Fund Project (GJJ170510).

References

1. Xu B, Qian D, Wang Z, Meng YS (2012) Recent progress in cathode materials research for advanced lithium ion batteries. Mater Sci Eng R 73:51–65
2. Chen J (2013) Recent progress in advanced materials for lithium ion batteries. Mater 6(1):156–183

3. Sun YK, Lee DJ, Lee YJ, Chen Z, Myung ST (2013) Cobalt-free nickel rich layered oxide cathodes for lithium-ion batteries. Acs Appl Mater Inter 5(21):11434–11440
4. Kang J, Han B (2015) First-principles study on the thermal stability of $LiNiO_2$ materials coated by amorphous Al_2O_3 with atomic layer thickness. Acs Appl Mater Inter 7(21):11599–11603
5. Liang CP, Kong FT, Longo RC, KC S, Kim JS, Jeon SH, Choi S, Cho K (2016) Unraveling the origin of instability in Ni-rich $LiNi_{1-2x}Co_xMn_xO_2$ (NCM) cathode materials. J Phys Chem C 120(12): 6383–6393
6. Hwang S, Kim SM, Bak SM, Kim SY, Cho BW, Chung KY, Lee JY, Stach EA, Chang WY (2015) Using real-time electron microscopy to explore the effects of transition-metal composition on the local thermal stability in charged $Li_xNi_yMn_zCo_{1-y-z}O_2$ Cathode Materials. Chem Mater 27(11):3927–3935
7. Konishi H, Yoshikawa M, Hirano T (2013) The effect of thermal stability for high-Ni-content layer-structured cathode materials, $LiNi_{0.8}Mn_{0.1-x}Co_{0.1}Mo_xO_2$ (x =0, 0.02, 0.04). J Power Sources 244(4):23–28
8. Dianat A, Seriani N, Bobeth M, Cuniberti G (2013) Effects of Al-doping on the properties of Li–Mn–Ni–O cathode materials for Li-ion batteries: an ab initio study. J Mater Chem A 1(32):9273–9280
9. Zhang B, Li L, Zheng J (2012) Characterization of multiple metals (Cr, Mg) substituted $LiNi_{0.8}Co_{0.1}Mn_{0.1}O_2$ cathode materials for lithium ion battery. J Alloy Comp 520:190–194
10. Lyu YC, Zhao NJ, Hu EY, Xiao RJ, Yu XQ, Gu L, Yang XQ, Li H (2015) Probing reversible multielectron transfer and structure evolution of $Li_{1.2}Cr_{0.4}Mn_{0.4}O_2$ cathode material for Li-ion batteries in a voltage range of 1.0–4.8 V. Chem Mater 27(15):5238–5252
11. Bak SM, Hu E, Zhou Y, Yu X, Senanayake SD, Cho SJ, Kim KB, Chung KY, Yang XC (2014) Structural changes and thermal stability of charged $LiNi_xMn_yCo_zO_2$ cathode materials studied by combined in situ time-resolved XRD and mass spectroscopy. Acs Appl Mater Interfaces 6(24):22594–22601
12. Zhao T, Chen S, Chen R, Li L, Zhang X, Xie M, Wu F (2014) The positive roles of integrated layered-spinel structures combined with nanocoating in low-cost Li-rich cathode $Li[Li_{0.2}Fe_{0.1}Ni_{0.15}Mn_{0.55}]O_2$ for lithium-ion batteries. Acs Appl Mater Interfaces 6(17):21711–20720
13. Li Q, Li G, Fu C, Luo D, Fan J, Li L (2014) K^+-doped $Li_{1.2}Mn_{0.54}Co_{0.13}Ni_{0.13}O_2$: a novel cathode material with an enhanced cycling stability for lithium-ion batteries. Acs Appl Mater Interfaces 6(13):10330–10341
14. Augustyn V, Therese S, Turner T, Manthiram A (2015) Nickel-rich layered $LiNi_{1-x}M_xO_2$ (M = Mn, Fe, and Co) electrocatalysts with high oxygen evolution reaction activity. J Mater Chem A 3(32): 16604–16612
15. Schipper F, Dixit M, Kovacheva D, Talianker M, Haik O, Grinblat J, Erickson EM, Ghanty C, Major DT, Markovsky B, Aurbach D (2016) Stabilizing nickel-rich layered cathode materials by a high-charge cation doping strategy: zirconium-doped $LiNi_{0.6}Co_{0.2}Mn_{0.2}O_2$. J Mater Chem A 4(41):16073–16084
16. Cho J (2000) $LiNi_{0.74}Co_{0.26-x}Mg_xO_2$ cathode material for a Li-ion cell. Chem Mater 12(10):3089–3094
17. Dou S (2013) Review and prospect of layered lithium nickel manganese oxide as cathode materials for Li-ion batteries. J Solid State Electrochem 17:911–926
18. Boulineau A, Simonin L, Colin JF, Canévet E, Daniel L, Sébastien P (2012) Evolutions of $Li_{1.2}Mn_{0.61}Ni_{0.18}Mg_{0.01}O_2$ during the initial charge/discharge cycle studied by advanced electron microscopy. Chem Mater 24(18):3558–3566
19. Zhang Y, Wang ZB, Lei J, Li FF, Wu J, Zhang XG, Yu FD, Ke K (2015) Investigation on performance of $Li(Ni_{0.5}Co_{0.2}Mn_{0.3})_{1-x}Ti_xO_2$ cathode materials for lithium-ion battery. Ceram Int 41(7):9069–9077
20. Kam KC, Mehta A, Heron JT, Doeff MM (2014) Electrochemical and physical properties of Ti substituted layered nickel manganese cobalt oxide (NMC) cathode materials. J Electrochem Soc 159(8): A1383–A1392
21. Liu H, Li J, Zhang Z, Gong Z, Yang Y (2004) Structural, electrochemical and thermal properties of $LiNi_{0.8-y}Ti_yCo_{0.2}O_2$ as cathode materials for lithium ion battery. Electrochim Acta 49(7):1151–1159
22. Yi TF, Yin LC, Ma YQ, Shen HY, Zhu YR, Zhu RS (2013) Lithium-ion insertion kinetics of Nb-doped $LiMn_2O_4$ positive-electrode material. Ceram Int 39(4):4673–4678
23. Yi TF, Xie Y, Zhu YR, Zhu RS, Ye MF (2012) High rate micron-sized niobium-doped $LiMn_{1.5}Ni_{0.5}O_4$ as ultra high power positive-electrode material for lithium-ion batteries. J Power Sources 211:59–65
24. Wu JF, Liu HH, Ye XH, Xia JP, Lu Y, Lin CW, Yu XW (2015) Effect of Nb doping on electrochemical properties of $LiNi_{1/3}Co_{1/3}Mn_{1/3}O_2$ at high cutoff voltage for lithium-ion battery. J Alloy Comp 644:223–227
25. Li X, Xin HX, Liu YF, Li D, Yuan XQ, Qin XY (2015) Effect of niobium doping on the microstructure and electrochemical properties of lithium-rich layered $Li[Li_{0.2}Ni_{0.2}Mn_{0.6}]O_2$ as cathode materials for lithium ion batteries. Rsc Adv 5(56):45351–45358
26. Gao Y, Wang X, Ma J, Wang Z, Chen L (2015) Selecting substituent elements for Li-rich Mn-based cathode materials by density functional theory (DFT) calculations. Chem Mater 27(9):3456–3461
27. Kong F, Longo RC, Park MS, Yoon J, Yeon DH, Park JH, Wang WH, KC S, Doo SG, Cho K (2015) Ab initio study of doping effects in $LiMnO_2$ and Li_2MnO_3 cathode materials for Li-ion batteries. J Mater Chem A 3(16):8489–8500
28. Li Z, Chernova NA, Feng J, Upreti S, Omenya F, Whittingham MS (2012) Stability and rate capability of Al substituted lithium-rich high-manganese content oxide materials for Li-ion batteries. J Electrochem Soc 159(2):A116–A120
29. Li Y, Han Q, Ming X, Ren M, Li L, Ye W, Zhang X, Xu H, Li L (2014) Synthesis and characterization of $LiNi_{0.5}Co_{0.2}Mn_{0.3}O_2$ cathode material prepared by a novel hydrothermal process. Ceram Int 40(9):14933–14938
30. Li J, Tian Y, Xu C (2012) Influence of Nb^{5+} doping on structure and electrochemical properties of spinel $Li_{1.02}Mn_2O_4$. J Mater Sci Technol 28(9):817–822
31. Zhao R, Yang Z, Chen JC, Chen Z, Liang J, Chen H (2015) Novel solvo/hydrothermal assisted co-precipitation method for faceted $LiNi_{1/3}Mn_{1/3}Co_{1/3}O_2$ cathode material. J Alloy Comp 627:206–210
32. Hashem AMA, Abdel-Ghany AE, Eid AE, Trottier J, Zaghib K, Manger A, Julien CM (2011) J Power Sources 196(20):8632–8637
33. Zhong S, Lai M, Yao W, Li Z (2016) Synthesis and electrochemical properties of $LiNi_{0.8}Co_xMn_{0.2-x}O_2$ positive-electrode material for lithium-ion batteries. Electrochim Acta 212:343–351
34. Zhong S, Chen P, Yao W (2015) Ni-rich layered oxide $Li_{1.05}(Ni_{0.7}Mn_{0.3})O_2$ as a highly reversible cathode material for lithium-ion batteries. Ecs Electrochem Lett 4(6):A45–A48
35. Zhen C, Jin W, Chao DL, Baikie T, Bai LY, Chen S, Zhao YL, Sum TC, Lin JY, Shen ZX (2016) Hierarchical porous $LiNi_{1/3}Co_{1/3}Mn_{1/3}O_2$ nano-/micro spherical cathode material: minimized cation mixing and improved Li^+ mobility for enhanced electrochemical performance. Sci Rep 6:25771–25780
36. Li LJ, Li XH, Wang ZX, Guo HJ, Yue P, Chen W, Wu L (2011) A simple and effective method to synthesize layered $LiNi_{0.8}Co_{0.1}Mn_{0.1}O_2$ cathode materials for lithium ion battery. Powder Technol 206(3):353–357
37. Kim D, Lim JM, Lim YG, Yu JS, Park MS, Cho M, Cho K (2015) Design of nickel-rich layered oxides using d electronic donor for redox reactions. Chem Mater 27(18):6450–6456
38. Zhang J, Lu QW, Fang JH, Wang JL, Yang J, NuLi YN (2014) Polyimide encapsulated lithium-rich cathode material for high voltage lithium-ion battery. Acs Appl Mater Interfaces 6(20):17965–17973